Revised Mapping of Lava Flows on Mt. Etna, Sicily

Michael Abrams*, Remo Bianchi**, David Pieri*

*Jet Propulsion Laboratory/California Institute of Technology
Mail Stop 183-501
4800 Oak Grove Dr.
Pasadena, CA 91109

**CNR Progetto LARA
Via Monte D'Ore, 11
00040 Pomezia, Italy

ABSTRACT

Mt. Etna, Sicily is the most active volcano in Europe, erupting almost constantly. Historical records of eruptions for the last 350 years are accurate; prior to about 1650, the record is increasingly inaccurate and incomplete. Ages for pre-1650 lava flows, reported on recent geologic maps, are in conflict. with ages determined from paleomagnetic measurements . Here we report on a different approach used to determine relative ages of Etnean flows. Multispectral image data were acquired from aircraft overflights of Etna in 1991. 'I'he Thematic Mapper Simulator instrument. used obtains 12 channels of data in the visible through thermal infrared wavelength regions. Supervised classification of these data allowed us to group Etnean flows into age groups based on their spectral properties. About 90% of the classification agrees with the mapped flow ages. Our results also generally support the paleomagnetic age determinations for flow ages that disagree with the mapped ages. In addition, several areas were remapped, correcting errors on the published map.

1. INTRODUCTION

Mount Etna is a composite volcano, about 40 km in basal diameter, that lies in the eastern part of Sicily, close to the probable position of the junction between the African and Eurasian plates (Figure 1) . Rising to an elevation of over 3300 m, and dominating the landscape of the Mediterranean region, the volcano is almost continuously active, and historical accounts of eruptions go back more than 2500 years (Chester, *et al.,* 1985) . Etnean lavas from major eruptions during the past 350 years are well known and documented. Contrary to popular ideas, however, eruptions from before about 1650 are poorly described, and the descriptions and attributed ages are often inaccurate. For example, for the period between 1300-1600, only three eruptions can be identified with a reasonable level of confidence (Tanguy *et al .,* 1985), although many eruptions are assigned to this period, and are so shown on the latest geologic maps of Etna (Romano, *et al.*, 19'/9; Romano, 1990) .

An accurate knowledge of the true dates of Etnean lavas has implications for the succession of eruptions, effusion rates, magmatic evolution, and eruptive models in general (Casetti, *et al.*, 1981, for example) . The direct method to obtain this knowledge is through C-14 dating of charcoal samples reliably associated with each flow. Unfortunately, finding this material has proved logistically difficult, requiring a field search of over 1700 km^2. Intensive research into existing historical records has also proved less than satisfactory (Tanguy, 1981), due to both the inaccuracy and incompleteness of written accounts.

One solution in the past 20 years has been to try to date Etnean flows through paleomagnetic analyses. This is done by determining the natural remnant magnetization of the flows, constructing curves which show the local secular variation of the field in both direction and magnitude, then finding the values of the flows on these curves. The first person to do this for Etnean lavas was Tanguy (1970) and Tanguy *et al.*, (1985); a similar analysis was done later by Rolph, *et al*. (1987). Tanguy examined about 30 flows, and found that most of the flows reported to have been erupted between AD 1284 and 1651 were actually older than this period, sometimes by more than 500 years. Rolph and his colleagues looked at about 40 flows, many of them being the same as those examined by Tanguy. Their results generally confirmed Tanguy's conclusions for the 1284–1651 period flows; paleomagnetic ages for 8 flows were many hundreds of years older than their mapped ages.

In this paper, we present the results of a different approach to determine relative ages of lava flows through the use of remote sensing data. Multispectral image data in the visible, near infrared (NIR), short wavelength infrared (SWIR), and thermal infrared (TIR) wavelength regions can obtain reflectance and emittance information for all areas in the image data set, with spatial. resolutions dependent on the instrument, and the platform altitude. Previous studies (Kahle, *et al.*, 1988; Abrams, *et* al., 1991) have demonstrated the use of optical and thermal aircraft data for relative age dating of lava flows in Hawaii . These data are sensitive to variations in vegetation type and percent cover; iron oxidation state of the surface; development of secondary coatings; and physical state of the surface. All of these factors vary as a function of age; in addition, climatic environment and human activities play a role in modifying the lava surface characteristics.

We report here on a study to map the relative ages of Etnean lava flows using aircraft remote sensing data. One of our principal objectives was to evaluate and, if confirmed, extend the results from the paleomagnetism studies, including flows older than those studied by Tanguy and Rolph *et al.*

2. ERUPTIVE HISTORY

The eruptive history of Etna from about 150,000 BP to the present has been characterized by products of mildly alkalic affinity, the Alkalic Series, and the main construct of the volcano is composed of basic lavas (hawaiites, mugearites, benmoreites) and rare trachytes. The lavas are typically porphyritic with phenocrysts of plagioclase, calcic augite and olivine, but some of the more evolved products are aphanitic. The more evolved products are all prehistoric in age, while over the last 100,000 years, only rather uniform hawaiitic composition lavas have been erupted (Chester *et al.*, 1985) .

Also, during historical time most of the eruptions have been effusive with explosive strombolian activity building cinder-cones over the vents in some cases. The summit region is characterized by almost continuous activity including lava effusions, strombolian explosions and pit collapses. This activity on Etna is referred to as "persistent" and is taken to indicate that the central conduit has been "open" for much of historical. time (Romano, 1982b) . Flank eruptions occur on average about every six years as a result of dikes from the central conduit intersecting the surface. Preferred locations for such eruptions are the north-east and southernrifts, small- loci of activity on the west flank, low on the southern flank and on the northern margin of the Vane del Bove (Guest, 1982) . Most of the lavas are aa but some pahoehoe flow fields have been produced in historical times.

Over much of the area of the volcano, slopes are shallow with a concave profile, but above about 1800 m they steepen to 20 degrees or more (Guest , 198'2) . The break in the slope represents the contact between the Piano Caldera and the Summit Cone. Much of the surface of the volcano is covered with lavas erupted during the last 5,000 years, but dating of historic material starts from 693 BC. Except for areas traversed by recent flows, the volcano's flanks are vegetated up to about 2,000 m a.s.l. Above this elevation there are only sparse vegetation, lavas erupted during the last few hundred years, and scoria and ash deposits produced by summit strombolian activity. The degree of vegetation cover on historical lavas depends not only on their age but also on altitude and sector of the volcano on which they lie.

The geology of Mount Etna is illustrated by a 1:50,000 scale geological map which includes historical lavas up to 1974 (Romano et al., 1979), and by the recent 1:60,000 scale naturalistic map (Figure 2) which describes the geology up to the 1990 activity (Romano, 1990) . There are two general. reviews which provide a detailed summary of current understanding of the volcano (Romano [Editor], 1982a; Chester *et al.*, 1.985).

3. DATA AND PROCESSING

The remote sensing data base for this study was acquired with NASA's Thematic Mapper Simulator (TMS) multispectral scanner instrument. This instrument obtains 12 channels of 8-bit. data in the visible, near infrared (VNIR), short wavelength infrared (SWIR), and the thermal. infrared wavelength (TIR) regions (Table 1). The two thermal channels cover the same wavelength region, differing only in the gain factor; only one was used during this study. The instrument was flown aboard NASA's ER-2 aircraft at an altitude of 20 km above sea level, on July 19, 1991. Three parallel, overlapping north-south lines of data were flown, about 20 minutes apart. The TMS scans the ground with a field of view of 42.5°, and an instantaneous field of view of 1.'25 mrad. Thus the data have a spatial resolution (pixel. size) of 25 m at sea level, and the swath width is 15.4 km. For targets above sea level., the spatial resolution and swath width are less: at the summit of Etna, the pixel size is about 20 m.

The data were processed on a VAX computer using the VICAR image processing software. Pre-processing steps involved correction for variable atmospheric path length radiometric differences, and correction for the panorama effect due to the scan angle variation. The former problem manifests itself as a brightness gradient across the scene. It is due to a combination of factors, and is most pronounced at shorter wavelengths. 'The dominant. contribution is from Raleigh and Mie scattering from atmospheric aerosols. This adds both a multiplicative and additive term to the radiance recorded at the sensor, and is strongly dependent on the viewing geometry: the effect is most pronounced looking into the sun. In addition, there are artifacts introduced by the instrument looking at either sun-lit surfaces (at all scales) or at shadowed surfaces. We attempted to minimize this effect by flying the data near noontime in a north-south direction. Finally, there is a non-uniform contribution to the radiance due to the variable atmospheric thickness as a function of elevation.

While it is possible, in theory, to model all of these phenomena, and remove them from the data rigorously, no one in practice has succeeded in developing the complete formulation. The task is difficult from a modeling sense, and in addition, requires *in situ* measurements of optical opacity, aerosols, and vertical profiles of temperature, relative humidity, and aerosol. distribution. Most approaches reported in the literature have used empirical techniques to try to compensate for the larger effects to normalize the data (Otterman and Fraser, 1976; Kaufman and Joseph, 1982; Conel, *et.al*., 1985; Conel, 1990) .

We also used an empirical method to correct. our data. Each of the three scenes was averaged along the flight direction to produce a one-line average image. A straight line was fit to this average image for each channel; and these values were then subtracted from each line of data in the original scene. This method assumes that the average one-line image should be uniform, and any variation is due to the atmosphere.c effects. The magnitude of the correction ranged from 40 digital numbers (DN) to O DN for the VNIR channels, and 5 DN to O DN for the SWIR and TIR channels. Next, the data were corrected for the panorama distortion by resampling along each scan line to produce pixels representing equal areas on the ground.

The three radiometrically adjusted flight lines were mosai.eked together to produce a single data set. covering Mt. Etna . Mosaicking was done by registering each line to a Landsat Thematic Mapper (TM) image, itself registered to the] :50,000 topographic maps, and UTM projected. Tie points were identified between the TMS data and TM data; the tiepoint data set was used to construct a triangular tessellation grid; geometric transformations for each triangle were then computed to map the TMS data to the TM data. The data were resampled to a resolution of 14 m using cubic convolution; the three lines were then merged to produce the final. data set for spectral analysis.

Spectral analysis was done using a supervised classification technique, employing a Bayesian Maximum Likelihood classifier (Schowengerdt, 1983) (hereafter referred to as "the classification"). Training areas were defined on the image by manually outlining them on a computer screen. The size of the areas varied from 5 x 5 to 20 x 20 pixels. Several areas were selected for each of the classes, and statistics computed for each training class. The statistics consisted of the mean and standard deviation from each class, for each of the 1.1 channels of the TMS data. These statistical measures formed the basis for the Bayesian Classification. This algorithm examines every pixel in the scene, and assigns each to a class if its value (in a multispectral, n-dimensional sense) falls within the mean +2.5 standard deviation ellipsoid of one of the training classes. If the pixel's values fall outside one of the predefined classes, it is assigned to the class it is closest to, based on its Euclidean distance.

The results of the classification are displayed as a thematic map, where each class is assigned an arbitrary color, and all pixels belonging to that class are portrayed in that color (Figure 3) . In addition, to remove high frequency noise pixels, a smoothing filter was applied to the data, whereby an isolated pixel was reassigned to the class number of its most frequently occurring surrounding pixels, thus eliminating misclassifications due to noise, but also eliminating possible small (single pixel sized) areas.

Fifteen classes were used for the classification: two kinds of vegetation (dominantly shrubs, and mainly forests), clouds, city, sediments, pyroclastic rocks, and 9 ages of lava flows. We used existing published geologic maps to aid in selection of the training areas for historic lava flows and for the vegetation classes, with the exception of the "pyroclastic" class, whose training areas were defined from interpretation of contemporaneous air photos. Two types of pre-historic flows were defined by training areas, one with dominantly rock exposed (Historic + rock), the other with dominantly vegetation cover (Historic + vegetation) .

4 DISCUSSION

Overall, the results of the classification agreed very well with the 1990 geologic map; classification accuracy is over 90%. Some of the discrepancies are due to discontinuities in slopes and vegetation cover on the ground, and to lack of correction of image radiances for variable path radiance effects due to topography. On the classification map an abrupt change in classes also occurs at the seams between the three flight lines. These can be seen as vertical discontinuities located along UTM coordinates 491 and 500. (Note that locations are referenced to the UTM coordinate grid superimposed on the geologic map and classification, defining northing/casting) . They are due to radiometric discrepancies induced by viewing the same locations from opposite look directions at the extreme edges of the images. Other local problems are due to the presence of the gas and ash plume blowing south from the vents. The following discussion mainly focuses on the misclassifications with respect to the gee].ogjc map, and we present explanations for the differences between the geologic map and our classification map. We will also point out where we feel the geologic map is wrong, and show how our results compare with the paleomagnetism measurements. A summary of the age assignments of flows described in this section is found in Table 2.

The distributi.on of "pyroclasti c" deposits (red class) was checked by compari son with air photos acquired simultaneously with the TMS data. The classification map accurately depicts their general distribution at the time of data acquisition.

The “1951--1991” class (orange on Figure 3), composed of the youngest lava flows, is sharply defined on the classification map. All of these flows can easily be traced, including small details of flow tongues. Classification accuracy is near 100%, in that no flows of this age were assigned to another class, and no flows of other ages were assigned to this class.

The "1900-1950" class (melon colored) includes the 1910, 1911, 1923, and 1928 flows, of limited areal extent. The largest area of misclassification is that part of the 1892 flow (4167/501) is assigned to this class. Our class boundaries are arbitrarily selected at the end of centuries, while the spectral behavior forms a continuum; the 1892 flow is only 8 years older than 20th century flows, and so probably looks very similar spectrally. Another explanation for the misclassification of some areas of this flow can be related to the presence of the gas and ash plume that extended southward from the vent at the time of the data overflight, . Patchiness of the plume could contribute more or less atmosphere-c absorption to the path radiance. The fact that we can successfully separate 20th century flows into 2 classes suggests that chemical or physical changes of' the flow surfaces are occurring within a 100 year period, producing differences in the spectral responses.

The "1.9th" century class is depicted in magenta on Figure 3. Included in this age bracket are the 1.879, 1865, 1892, 1843, and 1.832 flows; the first two are properly classified with respect to the geologic map. Part of the 1.892 flow is classified with the 19(]0-1950 class, as discussed above. The 1843 flow (4180/488), except for its distal. end, is truly mist.lassifi.ed as 1.7th century. The 1832 flow (4183/490) is properly classified near its vent, but is misclassified as 18th century downhill. There is no obvious explanation for these true misclassifications, particularly since the paleomagnetic ages (Rolph et al., 1987) of these two flows are in agreement with their ages on the geologic map.

The "18th" century class is displayed in light pink. Included in this class are mapped flows from 1763, 1764, 1766, 1780 and 1792. The 1763 (4178/491), 1780 (4171/497), and 1792 (4172/505) flows are all. properly classified with respect to the geologic map. The 1764 flow (4183/497) is classified partly as 18th and mostly as 17th century; there are no paleomagnetism measurements for this flow. The age assignment is based on Sartorius' (1880) mention of eruption activity on the north flank of Etna, reported in the Benedictine archives in Catania, without any further details concerning the location or altitude of the flow. It is therefore possible that the 1764 date is incorrect. The 1766 flow (4173/501) is classified as 20th century; the misclassification may well be due to the presence of the gas and ash plume, similar to the 189'2 flow located in the same area.

The "17th" century class is displayed in dark blue. Two areas of the 1634–1638 flow (4171/504) and the 1651 west flow (41.81/490) are properly classified. Three flows, 161O (4175/497), 1614--1624 (4185/499), and 1646 (418"1/504), are classified correctly at their vents at higher elevations. Towards the middles of the flows occurs a major break in slope and associated change in the vegetation community. The downhill parts of these flows are assigned to younger classes by the classification; in addition, the distal end of the 1646 flow is classified as 16th century. We attribute the misclassification of the lower parts of the flows to the effects of vegetation change on the spectral signatures. The small 1689 flow (4177/51.0) is assigned to the "historical. + vegetation" class. It. is located on the wettest, most intensely cultivated eastern side of the volcano, and the original. surface has been severely impacted by humans. An area (4180/498) mapped as Ancient Mongibello has also been assigned to the 1.7th century class for its upper half, and "historical + vegetation" for its lower half. It is clear based on examinat.ion of air photos that there is a sharp contact between vegetated surfaces at lower elevations, and bare flows at higher elevations. The classification of the lower part agrees with its vegetated appearance on airphotos and mapped age as Ancient Mongibello, while the age of the upper part seems to be mis-dated on the geologic map, and may well be 17th century in age. To the south (4178/497) an area' mapped as 18th/19th century without a date appears in the 17th century class. Unfortunately, there are no paleomagnetic dates for this flow.provides no assistance in determi.ni.ng its age. It also may properly belong to the 17th century in age. Near 4181./502 appear several elongate islands of older flows (kipukas) classified as 17th century; these areas are not defined on the geologic map, and occur within large mapped areas of Ancient Mongibello. The 1651 flow on the east is classified as both 16th century and 1951-1991. Rolph *et al.*'s (1987) and Tanguy *et al.*,'s (1985) paleomagnetic measurements suggest an age between 800 and 1000 AD. On the ground, this flow is an anomalous pahoehoe flow, almost totally absent of' vegetation. This may explain why parts of it are incorrectly classified as most recent. The larger problem of the 16th century flows will be discussed in the next. section.

'I'he greatest. discrepancies between the dates appearing on the geologic map, and dates determined from paleomagnetic measurements are associated with all of the 16th century and some of the older flows. These include the large 1595 (4175/490), 1566 (4187/509), and 1536 (4188/494) flows, that appear in cyan on the classification map. Our classification groups these 3 flows together, along with parts of the 1651 east flow. The paleomagnetic dates (determined by Tanguy *et al.* (1985) are 1050-1250 for the 1595 and 1566 flows, and <1000 for the 1.536 and 1651 flows. Rolph *et al_.* (1987) suggest dates of 1169 for the 1595 flow, late 14th century for the 1566 flow, 1536 for the 1536 'flow, and 800–1000 for the 1651 flow. Our classification results, while they do not allow assignment of these flows to a particular age, support the uniformity of their ages as presented by Tanguy's work. Spectrally they appear similar, suggesting that their ages are restricted to a relatively small time interval; i.e., 1000-1200.

A good example of the use of the classification map to revi se the geologic, map is found on the west flanks of Etna (4173/491) . The geologic map (Figure 4a) shows flows of three ages: 1610, 1607, and 1595. The geologic map shows the 1607 and 1610 flows as two distinct eruptions. In fact, Tanguy (1981) demonstrates that the historical record is in error, and both flows are from the same 1610 eruption. The distal end of this flow is called the "Lava Grande". Based on our image results, our classification assigns this part of the flow to "historical + vegetation" class, and not to the 1610 flow. To resolve this ambiguity, we investigated the distribution and interrelate.onsl)ips of these flows in the field. We found that the down-slope part of the 1610 flow consisted of thin flows sitting on top of very old flows; their areal extent was greatly subordinate to the underlying old materials. Using color infrared airphotos as a base, and our image results and field observations as a guide, we produced a new map of this area (Figure 4b), showing the more restricted extent. of the 161.0 flow; the presence of a "younger prehistoric flow" underneath it, and the "older prehistoric" flows. (The last two are included in our image class "historic+vegetation".) It was primarily the image classification results that. alerted us to the discrepancy between the mapped geology and the actual field relations.

Finally we come to the 812?-1169? flow (4165/49'/), displayed in gray on the classification map. Tanguy (1970;

1981), based on paleomagnetism and research of historic documents, assigns it to about 1000 AD. The classification indicates that this flow is spectrally unique: it was not assigned to any other class when no training areas were selected within it; and no other flows were assigned to its class when training areas were defined for it. Thus, even after our attempt at multispectral classification, its true age remains problematic.

5. CONCLUSION

The classification map of Etnean volcanic materials, produced from airborne Thematic Mapper Simulator data, has allowed us to resolve some of the discrepancies between flow ages shown on the published geologic maps, and flow ages determined from paleomagnetic measurements. The majority of the classification results confirms the mapped ages of lava flows . In a few areas, the classification has allowed us to redraw the geologic relations that were incorrectly depicted on the map. The classification supports Tanguy's paleomagnetic assignment of ages for the mapped 16th century flows as all having been erupted in the same time period, rather than different time periods as proposed by Rolph's work. We also discovered several areas that our classification assigned to particular ages, where the map showed either ancient- flows or the outcrop patterns were entirely missing.

Most of the differences between the published and the classification maps were due to errors on the published map, and not due to classification errors. Based on these results, remote sensing data, used jointly with field mapping and examination of air photos, represents a powerful tool for improving geologic mapping of volcanic rocks, even for a volcano as well studied and mapped as Mt.. Etna.

6. ACKNOWLEDGMENTS

Work done by Abrams and Pieri was performed at the Jet Propulsion Laboratory, California Institute of Technology, under contract to the Nationa]. Aeronautics and Space Administration . Wørk done by Bianchi was performed at the CNR Area Ricerca Frascati, Italy.

7. REFERENCES

Abrams, M., Abbott, E., Kahle, A., 1991, Combined use of visible, infrared, and thermal infrared images for mapping Hawaiian lava flows, *Journal of Geophysical Research,* 96, 475-484.

Casetti, G., Frazzetta, G., Romano, R., 1981, A statistical analysis in time of the eruptive events on Mount Etna (Italy) from 1323 to 1980, Istituto Internazionale di Vulcanologia, Consiglio Nazionale delle Ricerche, Publication 154.

Chester, D., Duncan, A., Guest, J., Kilburn, C., 1985, *Mount Etna* (Stanford, California: Stanford University Press).

Conel, J., 1990, Determination of surface reflectance and estimates of atmospheric optical depth and single scattering albedo from Landsat Thematic Mapper data, *International Journal of Remote Sensing,* **11**, *783--828.*

Conel, J., Lang, H., Paylor, E., Alley, R., 1985, Preliminary spectral and geologic analysis of Landsat-4

Thematic Mapper, Wind River Basin area, Wyoming, *IEEE Trans. on Geoscience and Remote Sensing*, GE-23, 562–573.

Guest, J. E., 1982, Styles of eruption and flow morphology on Mt.Etna, in *Mount. Etna Volcano: a Review of Recent Earth Science Studies* (cd. R. Romano), Mem. Sot. Geol . Italy, 23, 49-73.

Kahle, A., Gillespie, A., Abbott, E., Walker, R., Hoover, G., Lockwood, J., 1988, Mapping and relative age dating of Hawajian basalt flows using multispectral thermal infrared images, *Journal. of Geophysical Research,* 93, 15,'239-15,251.

Kaufman, Y., and Joseph, J., 1982, Determination of surface albedos and aerosol extinctions coefficients from satellite imagery, *Journal of Geophysical Research, 87, 1287–1299.*

Otterman, J., and Fraser, R., 1976, Earth-atmosphere system and surface refl.activities in arid regions from Landsat MSS data, *Remote Sensing of Environment,* **5**, 24"1--266.

Rolph, T'., Shaw, J., Guest, J., 3.98-/, Geomagnetic field variations as a dating tool: application to Sicilian lavas, *Journal of Archaeological Science,* 14, 21.5--225.

Romano, R. (editor), 1982a, *Mount Etna Volcano: a Review of Recent Earth Science Studies* (cd. R. Romano) , Mere. Sot. Geol. Italy, 23.

Romano, R., 1982b, Succession of the Volcanic Activity in the Etnean Area, in *Mount Etna Volcano: a Review of Recent Earth Science Studies* (cd. R. Romano), Mere. Sot. Geol_. Italy, 23, 27-48,

Romano, R., 1990, *Mt. Etna: carta naturalistica e turistica,* Societa elaborazione cartografiche and Club Alpino Italiano, 1:60,000, Florence, Italy.

Romano, R., Sturiale, C., Lentini, F., et al., 1979, *Carta Geologica del Monte Etna*, Consiglio Nazionale delle Ricerche Progetto Finalizatto Geodynamica, 1:50,000, Catania, Sicily.

Sartorius Von Waltershausen, W., 1880, *Der Aetna, 2* vol . publ . par von Lasaulx, W.' Engelman, Leipzig.

Schowengerdt, R., 1983, *Techniques for Image Processing and Classification in Remote Sensing,* (New York: Academic Press) .

Tanguy, J., 1970, An archaeomagnetic study of Mount Etna: the magnetic direction recorded in lava flows subsequent to the twelfth century, *Archaeometry, 1.2, 115-128.*

Tanguy, J., 1981, Les éruptions historique de l'Etna: chronologies et localisation, *Bulletin of Volcanology, 44-3,* 585-640.

Tanguy, J., Bucur, 1., Thompson, J., 1985, Geomagnetic secular vari-ation in Sicily and revised ages of historic lavas from Mount Etna, *Nature,* 318, 453–455.

FIGURE CAPTIONS

1. Location map of Mount Etna in eastern Sicily, and general geology of Sicily (from Chester *et al.*, 1985)

2. Geologic map of Mt.. Etna, extracted from Romano (1990) . The grid overlay is 1 km UTM grid.

3. Bayesian Maximum Likelihood Classification map of Mt. Etna Thematic Mapper Simulator data. Classes represent 9 ages of lava flows, and 6 other classes of land cover types. The map covers an area of about 30 x 30 km . The grid overlay is 1 km UTM grid.

4. A) Published geologic map of an area on western flank of Mt. Etna (Romano, 1990). B) Revised geologic map for same area, based on interpretation of aircraft remote sensing data, airphotos, and field investigations.

Table 1. Thematic: Mapper Simulator Channels

CHANNEL	WAVELENGTH, μm	THEMATIC MAPPER BAND
1	0.42-0.45	
2	0.45-0.52	
3	0.52-0.60	
4	0.60-0.62	
5	0.63-0.69	
6	0.69-0.75	
7	0.76-0.90	
8	0.91.-1,.05	
9	1.55-1.75	
10	2.08-2.35	
11	8.5--14.0 (Low gain)	
12	8.5--14.0 (High gain)	

Table 2. Ages Attributed to Various Historical Lava Flows on Mt. Etna by Different Authors

This paper	Map (Romano, 1990)	Tanguy(1970)	Rolph et al. (1987)
1951-1991	1651E*	800-1000	800-1000
1900-1950	1910		
	1911		
	1923		
	1928		
	1892 (part)		
	1766*		
1800-1899	1879		
	1865		
	1892		
	1832 (near-vent)		
1700-1799	1763		
	1764 (partly)		
	1780		
	1792		
	1843*(proximal)		
	1832*(downhill)		
1600-1699	1634-1638		
	1651 E,W	<1000	800-1000
	1607	1610	
	1610	1610	
	1614-1624		
	1646 (higher elevations)		
	1843 *(distal)		
	1764 *(mostly)		
	Ancient Mongibello (upper half)		
	18th/1 9th century		
1500-1599	1646 *(distal end)		
1000-1200	1595	1050-1250	1169
	1566	1050-1250	>1350
	1536	<1000	1536
	1651E	<1000	800-1000
812?-1169?	812?-1169?	1000	

*misclassified in this paper

FIGURE CAPTIONS

1. Location map of Mount Etna in eastern Sicily, and general geology of Sicily (from Figure 3.'2, Chester *et al.*, 1985, modified for this report)

2. Geologic map of Mt. Etna, modified from Romano (1990). The grid overlay is 1 km UTM grid.

3. Bayesian Maximum Likelihood Classification map of Mt. Etna Thematic Mapper Simulator data. Classes represent 9 ages of lava flows, and 6 other classes of land cover types. The map covers an area of about 30 x 30 km. The grid overlay is 1 km UTM grid.

4. A) Published geologic map of an area on western flank of Mt. Etna (modified from Romano, 1990). B) Revised geologic map for same area, based on interpretation of aircraft remote sensing data, airphotos, and field investigations.

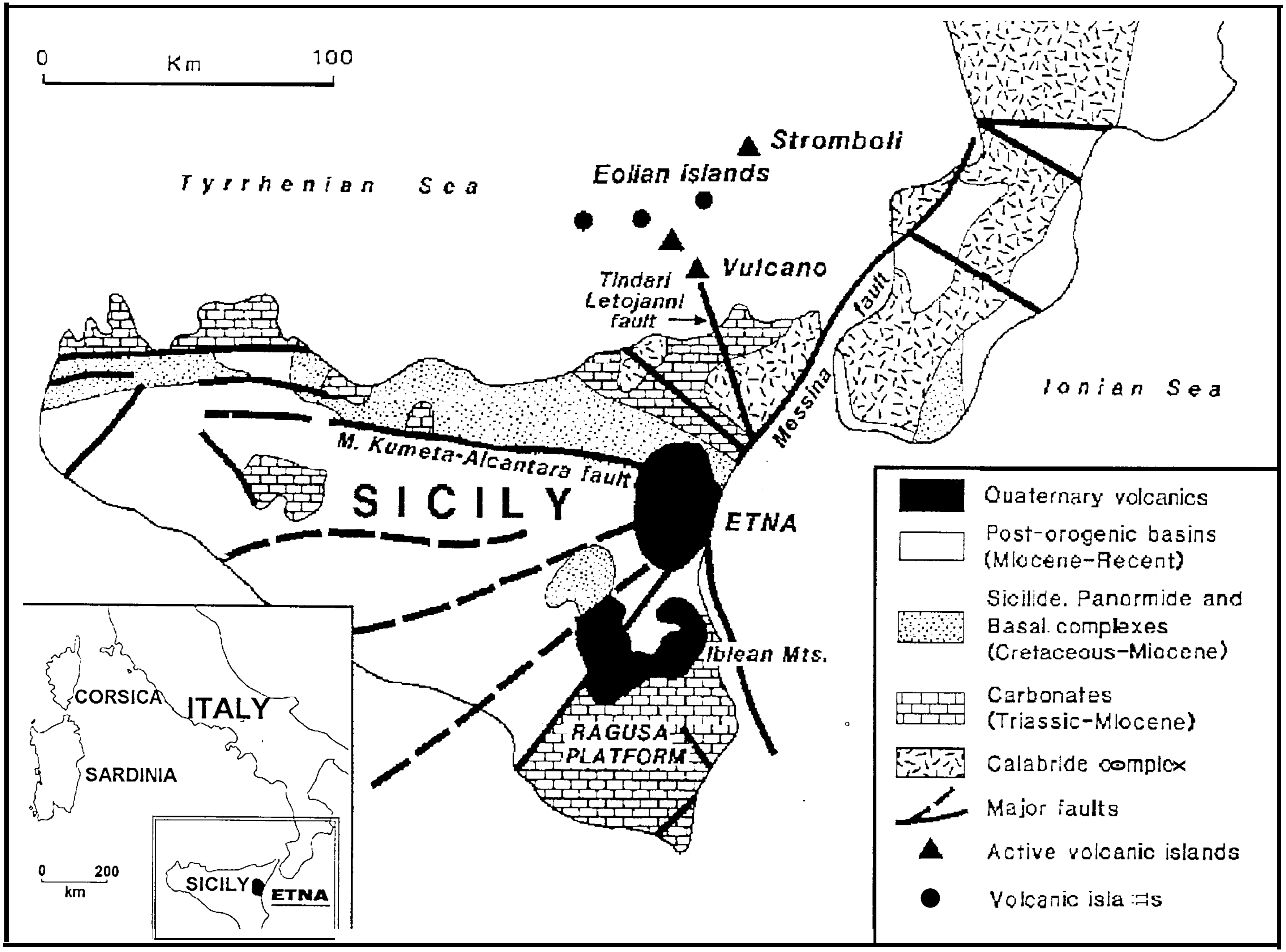
0 Km 100
Tyrrhenian Sea
Stromboli
Eolian islands
Vulcano
Tindari Letojanni fault
Messina fault
Ionian Sea
M. Kumeta-Alcantara fault
SICILY
ETNA
Iblean Mts.
RAGUSA PLATFORM
CORSICA
ITALY
SARDINIA
0 200
km
SICILY
ETNA
Quaternary volcanics
Post-orogenic basins (Miocene-Recent)
Sicilide. Panormide and Basal complexes (Cretaceous-Miocene)
Carbonates (Triassic-Miocene)
Calabride complex
Major faults
Active volcanic islands
Volcanic islands

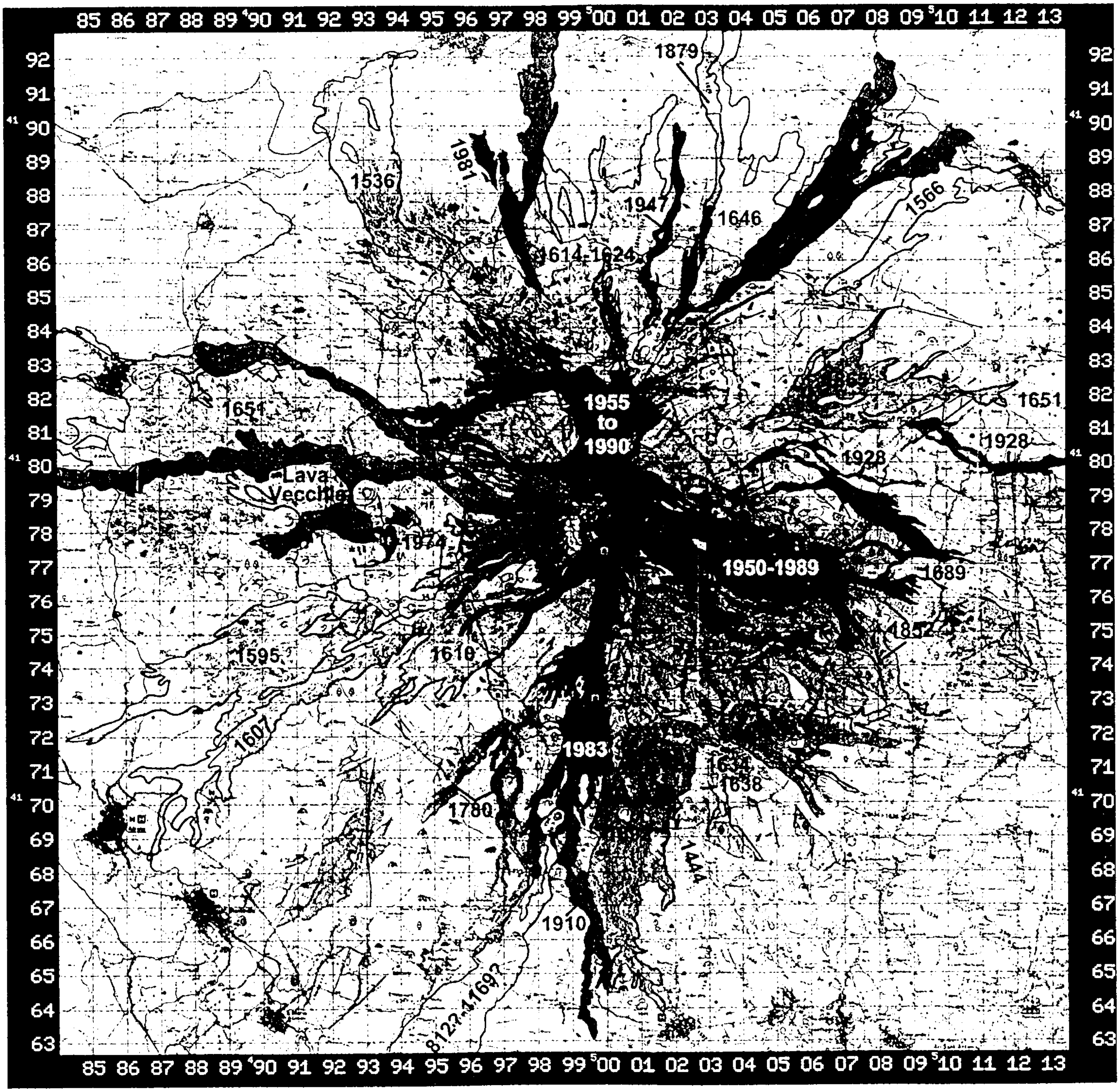
1879
1981
1536
1947
1646
1566
1614-1624
1955
to
1990
1651
1651
1928
1928
Lava
Vecchia
1974
1950-1989
1689
1852
1595
1610
1607
1983
1638
1780
1444
1910

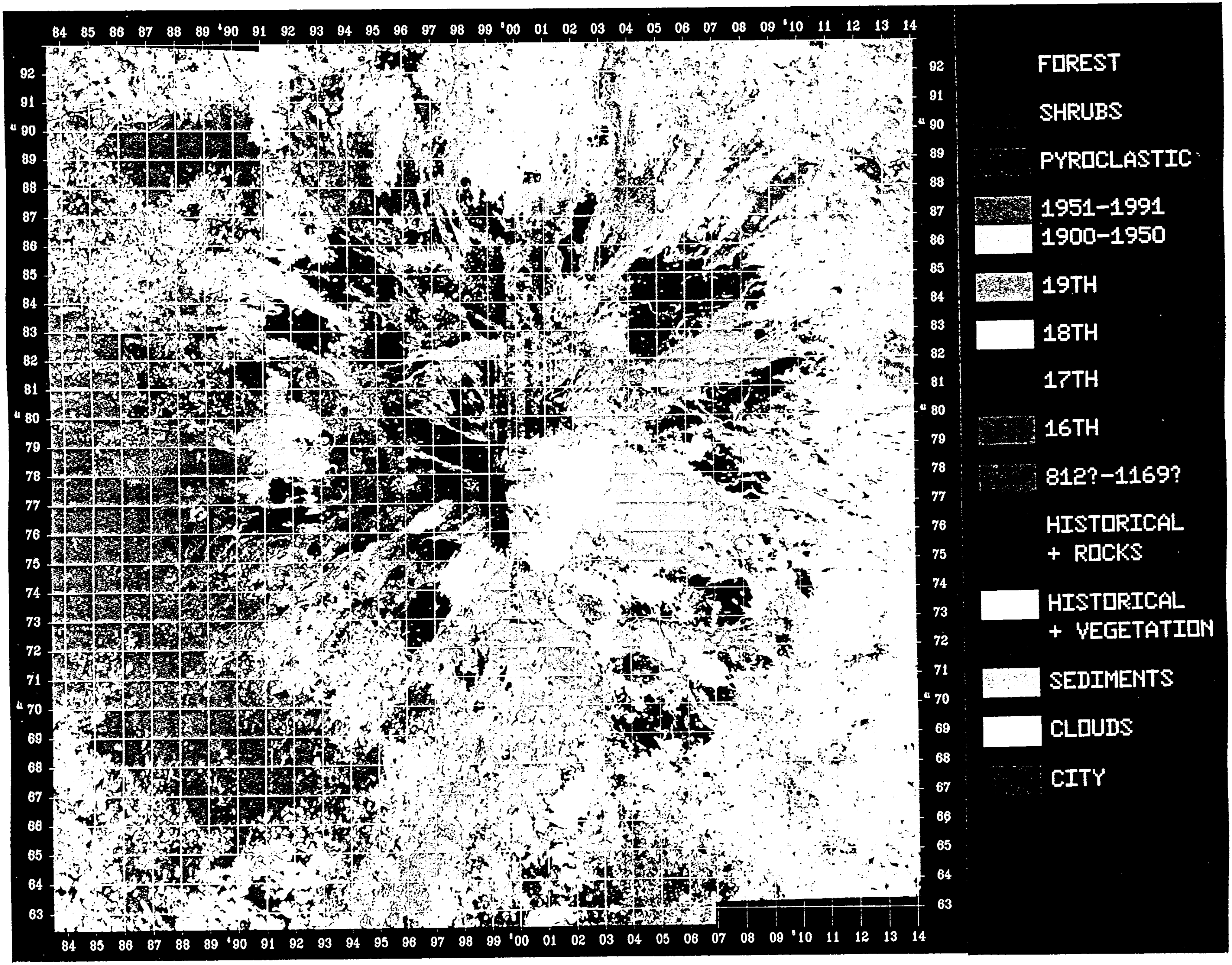
FOREST
SHRUBS
PYROCLASTIC
1951-1991
1900-1950
19TH
18TH
17TH
16TH
812?-1169?
HISTORICAL + ROCKS
HISTORICAL + VEGETATION
SEDIMENTS
CLOUDS
CITY

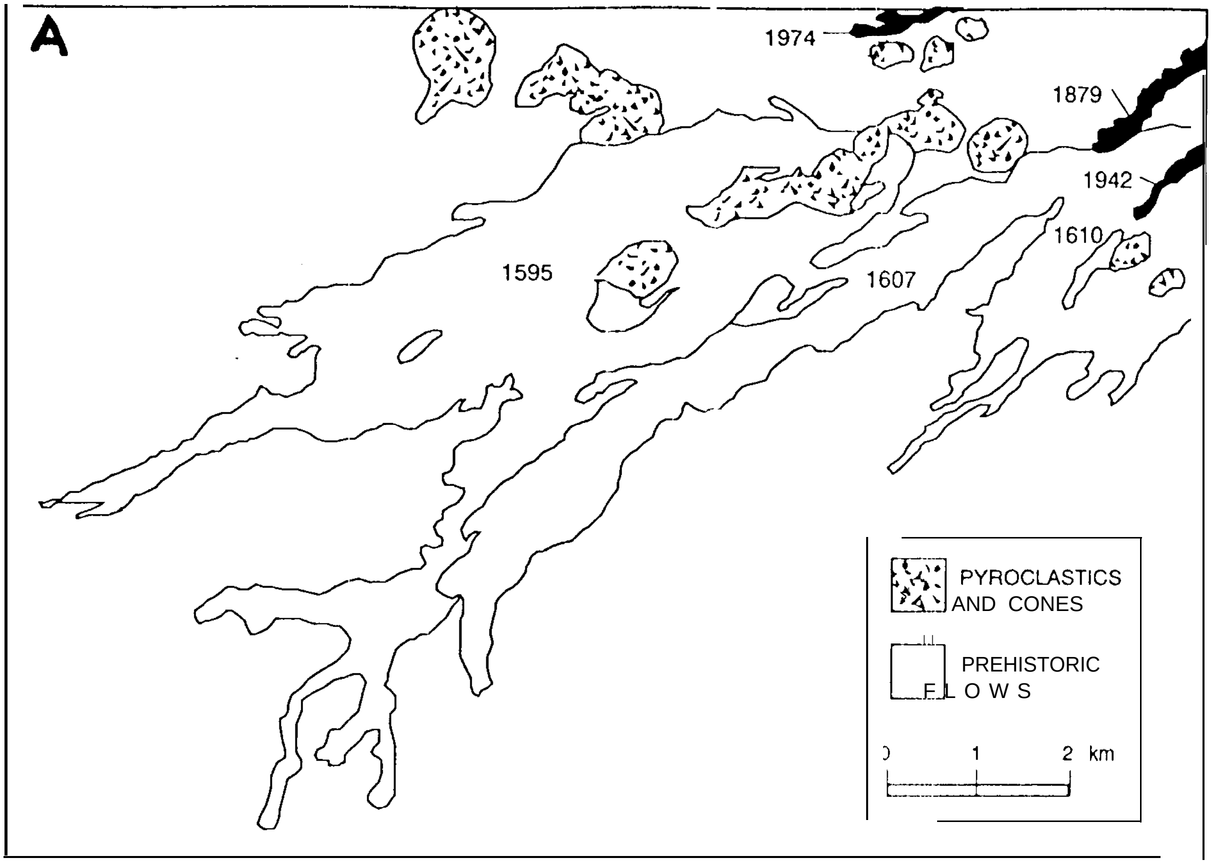
A
1974
1879
1942
1610
1595
1607
PYROCLASTICS AND CONES
PREHISTORIC FLOWS
0 1 2 km

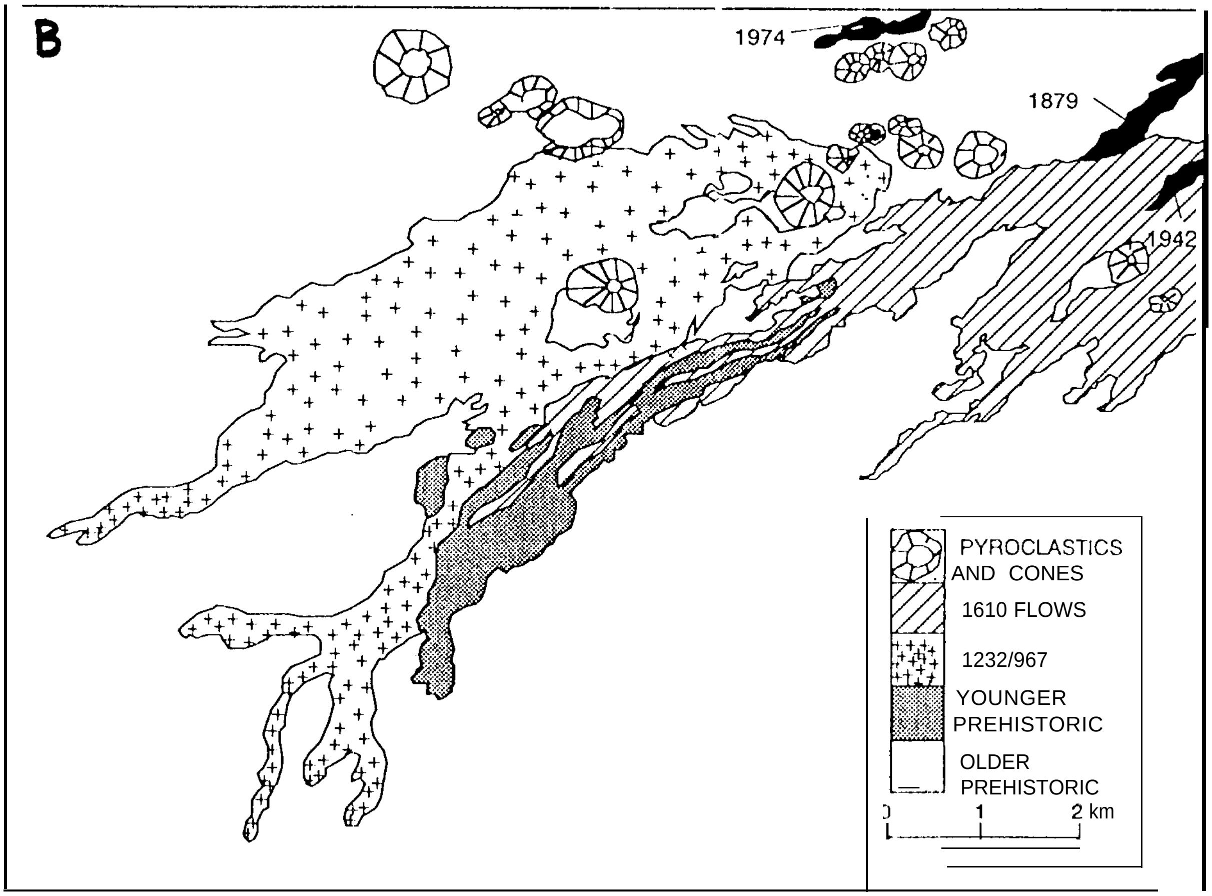
B
1974
1879
1942
PYROCLASTICS AND CONES
1610 FLOWS
1232/967
YOUNGER PREHISTORIC
OLDER PREHISTORIC
0 1 2 km